



## Perspective: Insight into reaction coordinates and dynamics from the potential energy landscape

D. J. Wales

Citation: [The Journal of Chemical Physics](#) **142**, 130901 (2015); doi: 10.1063/1.4916307

View online: <http://dx.doi.org/10.1063/1.4916307>

View Table of Contents: <http://scitation.aip.org/content/aip/journal/jcp/142/13?ver=pdfcov>

Published by the [AIP Publishing](#)

---

### Articles you may be interested in

Practical hyperdynamics method for systems with large changes in potential energy  
J. Chem. Phys. **141**, 234109 (2014); 10.1063/1.4903787

Guided ion beam and theoretical studies of the reaction of Ag + with CS<sub>2</sub>: Gas-phase thermochemistry of AgS + and AgCS + and insight into spin-forbidden reactions  
J. Chem. Phys. **132**, 024306 (2010); 10.1063/1.3285837

Revisiting the finite temperature string method for the calculation of reaction tubes and free energies  
J. Chem. Phys. **130**, 194103 (2009); 10.1063/1.3130083

The hydrogen abstraction reaction H + CH<sub>4</sub>. I. New analytical potential energy surface based on fitting to ab initio calculations  
J. Chem. Phys. **130**, 184314 (2009); 10.1063/1.3132223

Accurate ab initio potential energy surface, dynamics, and thermochemistry of the F + CH<sub>4</sub> → HF + CH<sub>3</sub> reaction  
J. Chem. Phys. **130**, 084301 (2009); 10.1063/1.3068528

---

A promotional graphic for the journal AIP APL Photonics. It features a stylized orange and yellow background with light rays. On the left, there is a thumbnail image of a journal cover showing a heatmap. To the right of the thumbnail, the text "Launching in 2016!" is written in large, bold, white letters. Below it, the text "The future of applied photonics research is here" is written in a smaller, white font. In the bottom right corner, the AIP APL Photonics logo is displayed.

# Perspective: Insight into reaction coordinates and dynamics from the potential energy landscape

D. J. Wales<sup>a)</sup>

*University Chemical Laboratories, Lensfield Road, Cambridge CB2 1EW, United Kingdom*

(Received 30 December 2014; accepted 11 March 2015; published online 1 April 2015)

This perspective focuses on conceptual and computational aspects of the potential energy landscape framework. It has two objectives: first to summarise some key developments of the approach and second to illustrate how such techniques can be applied using a specific example that exploits knowledge of pathways. Recent developments in theory and simulation within the landscape framework are first outlined, including methods for structure prediction, analysis of global thermodynamic properties, and treatment of rare event dynamics. We then develop a connection between the kinetic transition network treatment of dynamics and a potential of mean force defined by a reaction coordinate. The effect of projection from the full configuration space to low dimensionality is illustrated for an atomic cluster. In this example, where a relatively successful structural order parameter is available, the principal change in cluster morphology is reproduced, but some details are not faithfully represented. In contrast, a profile based on configurations that correspond to the discrete path defined geometrically retains all the barriers and minima. This comparison provides insight into the physical origins of “friction” effects in low-dimensionality descriptions of dynamics based upon a reaction coordinate. © 2015 AIP Publishing LLC. [<http://dx.doi.org/10.1063/1.4916307>]

## I. INTRODUCTION

The potential energy landscape perspective provides both a conceptual and a computational framework for molecular and condensed matter science.<sup>1</sup> The key components of this approach involve visualisation of the potential energy surface (PES) and tools for exploration of structure, dynamics, and thermodynamics. Many of these tools are based upon geometry optimisation, which allows us to connect the emergence of observable properties with the organisation of the underlying landscape. This approach is highly complementary to more conventional Monte Carlo (MC) and molecular dynamics (MD) techniques. In particular, it provides a framework to circumvent many difficulties associated with sampling problems arising from high potential energy barriers, which often lead to trapping, broken ergodicity, and rare event dynamics. The principal distinction between these methods and the huge variety of alternative approaches to enhanced sampling<sup>2–16</sup> and rare events<sup>17–20</sup> is the use of stationary points of the potential energy to provide an initial coarse-graining. Limits can be defined that permit either high accuracy or systematic approximations to be applied. It is not the purpose of this perspective to provide a review or critical comparison of all the possible approaches. However, efforts to benchmark different schemes are being actively pursued.<sup>21</sup>

Computationally, the potential energy landscape methodology can be divided into three connected categories, namely, structure prediction, thermodynamic sampling, and analysis of dynamics. In the present contribution, a brief overview of recent developments in each of these areas will first be presented (Sec. II). The contrast between the potential en-

ergy landscape formulation, which accounts for all degrees of freedom, and methods that require or extract a reaction coordinate to describe mechanism and dynamics is then developed. To connect these viewpoints, a new approach to sample a potential of mean force along geometrically determined pathways is then described in Sec. IV. The results provide a direct way to compare with calculations based on an order parameter that defines a reaction coordinate. The manifestation of the effects due to projection is then clear, and we see that in a benchmark system, even a relatively successful geometrical order parameter<sup>22</sup> averages over some of the barriers on the multidimensional path (Sec. V).

Sampling pathways defined by order parameters or reaction coordinates is a common approach for systems ranging from atomic clusters<sup>22</sup> to biomolecules.<sup>23–26</sup> Constrained sampling in hyperplanes,<sup>27</sup> or regions defined by Voronoi analysis,<sup>28</sup> has previously been used in conjunction with evolving pathways. In the present contribution, the reference path is defined by geometry optimisation and fixed. Such pathways form the basis of the computational potential energy landscape approach to approximate treatments of dynamics, and the present results suggest that they could be used to guide projection directly, if a reaction coordinate description is required. The methodology therefore provides a means to employ kinetic transition networks sampled within the framework of geometry optimisation for more accurate refinement of transition rates and analysis of rare events. The contributions of individual discrete paths, defined in terms of connected minimum-transition state-minimum triples,<sup>17</sup> to the overall rate can be estimated as a function of temperature, and more paths become significant as the temperature increases. This increase in entropy due to the number of relevant paths can be compared with the entropic contribution of the discrete paths themselves.

<sup>a)</sup>dw34@cam.ac.uk

The present approach may provide a way to account for anharmonic effects more accurately in this theoretical transition path framework.<sup>17,29–33</sup>

## II. OVERVIEW OF THE COMPUTATIONAL POTENTIAL ENERGY LANDSCAPE FRAMEWORK AND RECENT DEVELOPMENTS

### A. Basin-hopping global optimisation

Basin-hopping global optimisation employs steps between local minima on the potential energy surface.<sup>34–36</sup> Because a local minimisation is involved, large moves in configuration space can be proposed that may produce unphysical geometries, which are then rescued by geometry optimisation. A wide range of related schemes has been considered, mostly based upon alternative step-taking strategies and criteria for accepting and rejecting the resulting moves. Efficient minimisation is essential, and some of most popular methods have recently been compared systematically.<sup>37</sup> Physical insight into particular systems is likely to speed up the searches significantly if more productive moves in configuration space can be proposed,<sup>38</sup> and this approach is legitimate so long as it does not exclude any potentially important parts of the landscape.

For benchmark atomic clusters, which exhibit frustrated<sup>39,40</sup> multi-funnel<sup>41</sup> landscapes, efficiency gains of two to three orders of magnitude have been obtained by exploiting symmetrised moves.<sup>42</sup> This approach was inspired by the principle of maximum symmetry, which argues that structures with larger symmetry measures are more likely to have particularly high or particularly low energies.<sup>1,43</sup> The most useful scheme is probably a “core orbits” approach, where optimal arrangements of roughly symmetry equivalent atoms are sought within incomplete orbits of a core point group.<sup>42</sup>

Global optimisation for multicomponent materials, such as nanoalloys, must address the need to optimise with respect to both structure and chemical ordering. Using methods developed to solve graph partitioning problems, we have devised a deterministic method that outperforms conventional basin-hopping by orders of magnitude.<sup>44</sup> Focusing on biminima, defined as local minima in both coordinate and permutation space, facilitates even greater gains in efficiency.<sup>45</sup>

Less dramatic, but nevertheless useful, improvements have been realised by replacing the Boltzmann weight in the basin-hopping accept/reject step by a Tsallis weight.<sup>46</sup> Optimising an additional parameter in this weight reduced the mean first encounter time for the global minima by about a factor of 2 in test cases.<sup>47</sup> A theoretical basis for the value of the optimal parameter was also provided and matched the outcomes of numerical experiments very well.<sup>47</sup>

Significant efficiency gains for global optimisation in biomolecules can be obtained if large moves in configuration space can be proposed without causing groups of bonded atoms to overlap. Here, a group rotation scheme has been successfully applied,<sup>48–50</sup> and this approach can be combined with local rigidification of arbitrary sets of atoms,<sup>51</sup> using angle-axis coordinates.<sup>52,53</sup> For two peptides, where benchmarking statistics can still be obtained for less efficient approaches, local

rigidification improved the mean first encounter times for the global minima by up to a factor of 4. Much greater benefits are expected for larger systems, since the effective number of degrees of freedom is reduced, as well as the dimension of the search space and the cost of calculating the energy and gradient.

### B. Thermodynamic sampling

The superposition approach to thermodynamics provides an exact formulation, which forms the basis for convenient approximations that retain the key feature of explicit ergodicity.<sup>1,11,54–57</sup> The total density of states or partition function is written as a sum over the basins of attraction<sup>1,58,59</sup> of local minima. This method underlies several recent developments for enhanced sampling, as outlined below.

The superposition enhanced nested sampling (SENS) procedure<sup>60</sup> addresses a systematic failure of nested sampling,<sup>61</sup> where simulations become locked out of certain regions in configuration space that become disjoint below a particular energy threshold. SENS retains the strengths of the original nested sampling procedure, with the power of global optimisation to locate low-lying local minima efficiently. A reference set of minima is used in a Hamiltonian replica exchange method (HREM) scheme,<sup>62,63</sup> where moves are proposed between configurations sampled using different Hamiltonians. Specifically, minima are selected from the database according to their relative weights calculated using harmonic densities of states, in accord with a harmonic superposition approximation (HSA). Swaps are then considered between configurations sampled uniformly within the harmonic basin of attraction and a configuration sampled from the Hamiltonian in question under a certain energy constraint.<sup>60</sup> Convergence improvements up to a factor of about 20 were obtained for some benchmark atomic clusters.

The new basin-sampling procedure<sup>64</sup> provides much larger acceleration of sampling via an approximate treatment of the anharmonic vibrational density of states for the local minima. Again, the methodology exploits the fact that global optimisation can generally find all the relevant low-lying minima very quickly, even for frustrated landscapes<sup>39,40</sup> with competing morphologies. Basin-sampling combines knowledge of low-lying local minima with parallel tempering<sup>2,65</sup> to connect densities of states that are relevant in the low and high temperature regimes. A two-dimensional histogram of probabilities is constructed using the instantaneous potential energy and the energy of local minima obtained by regular quenching. An approximate anharmonic functional form is then fitted. This construction has the additional benefit that it can be employed to calculate the potential energy density of both local minimum structures and permutation-inversion isomers.<sup>64</sup>

The superposition framework is also exploited in the factorised superposition approach (FSA),<sup>50</sup> which provides a theory for the free energy change associated with non-covalent association of two molecules. It exploits our intuition that local molecular environments sufficiently distant from the interaction site are relatively unaffected by binding. Hence, it should not be necessary to sample the corresponding local configurations extensively. Convergence tests for binding of phenyl acetic acid to aldose reductase show that the free energy change

converges for factorisation of groups with about 80% of the protein rigidified.<sup>50</sup>

### C. Rare event dynamics

In this part of the computational potential energy landscape approach, the focus is on transition states and the pathways they mediate between local minima. Here, the transition states are defined geometrically as stationary points with a single negative Hessian eigenvalue.<sup>66</sup> Rate constants, mean first passage times, and committor probabilities are extracted<sup>67</sup> from the resulting kinetic transition network<sup>68–71</sup> for individual local minima or regrouped sets that define states with associated free energies.<sup>72–75</sup> Here, it is possible to exploit particular features of the network formulation to produce a graph transformation procedure that is much more robust than linear algebra methods.<sup>76</sup> The rate constants for individual minimum-to-minimum transitions can be estimated by any convenient unimolecular rate theory<sup>77</sup> or explicit dynamics. For the simplest harmonic normal mode approximations, the required metric tensor has now been derived for angle-axis coordinates,<sup>48</sup> which enables rates to be obtained for systems involving rigid body molecules and the general local rigidification scheme<sup>49,51</sup> within the discrete path sampling (DPS) framework.

Various methods to expand and refine a transition network<sup>69–71</sup> have been described within the general framework of DPS.<sup>17,29,30</sup> Details of all the geometry optimisation techniques involved have been described extensively in previous reports. For the comparison of free energy profiles discussed in Sec. IV, it is the approximate steepest-descent paths employed to define connections between local minima that are paramount.

Characterising an initial connected path between specified end point minima usually represents the first step to building the required network. Although this initial path is often kinetically irrelevant once a full network has been refined, it may not be straightforward to obtain the required connection. Particularly serious problems arise for some biomolecular systems where a naïve linear interpolation leads to unphysical chain crossings. The quasicontinuous interpolation scheme solves this problem by constructing an auxiliary potential that preserves the covalent bonding framework.<sup>78</sup> The method has now been applied successfully to proteins and nucleic acids. Our experience suggests that alternative methods, such as steered molecular dynamics, can produce pathways with barriers over an order of magnitude too large and reordering of fast and slow processes.

### D. Visualisation: Disconnectivity graphs

Three-dimensional surfaces with many local minima are often described as “rough” or “complex.” In fact, such pictures cannot faithfully represent a multi-dimensional potential energy surface. The number of local minima is expected to scale exponentially with the number of atoms,<sup>54,79,80</sup> and the average number of transition states per minimum is likely to scale linearly.<sup>80</sup> This connectivity usually means that three-dimensional surfaces correspond to a relatively small number of degrees of freedom.

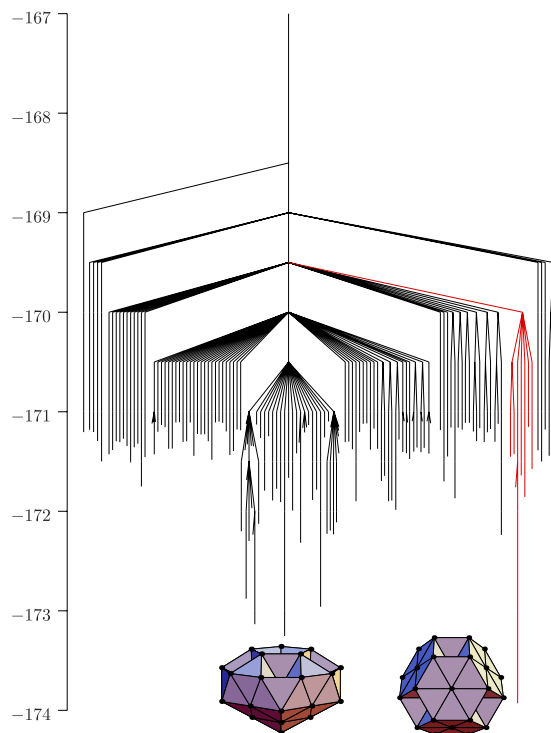


FIG. 1. Disconnectivity graph for the LJ<sub>38</sub> cluster, highlighting the competing morphologies that correspond to an incomplete Mackay icosahedron and a truncated octahedron. Branches of the graph corresponding to minima based on the octahedron (fcc packing) are coloured red. The vertical axis corresponds to potential energy in units of  $\epsilon$ .

For visualisation of landscapes in high-dimensional systems, the disconnectivity graph approach<sup>81,82</sup> has proved very insightful. In particular, universal principles have been recognised that connect atomic and molecular clusters, biomolecules, and soft and condensed matter with common self-organising properties. The corresponding organisation contrasts dramatically with the highly frustrated landscapes of glass-forming systems,<sup>52,71,83</sup> which exhibit an exponentially large number of low energy amorphous minima separated by high barriers. In the present contribution, the benchmark system for which free energy profiles are compared exhibits two principal competing morphologies, which correspond to a double funnel disconnectivity graph, illustrated in Figure 1. This structure produces two distinct time scales for relaxation to the global minimum, as well as a signature in the heat capacity corresponding to a low temperature solid-solid transformation.<sup>84</sup>

### III. REACTION COORDINATES AND PROJECTION

Experimental observables such as rate constants must be independent of the coordinates we may choose to describe the system. If our calculations account for all degrees of freedom, without introducing approximations, then coordinate independence can be achieved using covariant derivatives.<sup>85,86</sup> The choice of coordinate transformations in this context is then a matter of efficiency or convenience, for example, in changing the convergence of geometry optimisations.<sup>87,88</sup> It does not affect any calculated observables.

In contrast, the choice of a reaction coordinate, or any other projection from the full configuration space to a reduced space, is inherently approximate. Such projections can then be optimised in terms of how faithful they are in preserving the observable properties of interest for calculations in the reduced representation. Significant effort has been invested in this framework, especially for protein folding dynamics, where descriptions of the kinetics in terms of diffusion on a one-dimensional surface have often proved remarkably successful.<sup>89–91</sup> For example, a Bayesian approach has been used to variationally optimize coordinates by maximizing the conditional probability of being on a transition path for a certain value of the coordinate: this quantity has a theoretical upper bound for diffusive dynamics.<sup>92–94</sup> Alternatively, reproduction of committor probabilities,<sup>95</sup> often referred to as  $P_{\text{fold}}$  for proteins, along with hundreds of other structural and energetic variables, may be achievable by importance sampling combinations of many coordinates.<sup>96,97</sup> Committor probabilities and isocommittor surfaces feature in a variety of other studies,<sup>98–100</sup> and reaction coordinates have also been described for biochemical networks based on genetic switches.<sup>101</sup> Some schemes that aim to model rare events require reaction coordinates,<sup>102,103</sup> while other approaches extract them from simulation results.<sup>104–113</sup>

Reproducing folding rates provides an objective criterion for optimising the projection, although the resulting reaction coordinate(s) might depend on the observable(s) in question. In fact, different pathways in the same protein may correspond to different optimal combinations of coordinates,<sup>97</sup> and alternatives may be needed if a single coordinate is insufficient.<sup>28,114</sup> Focusing on a progress coordinate may also be helpful.<sup>115</sup>

Aside from possible physical insight, the search for a reaction coordinate can be motivated by the possibility of extracting dynamics using a low-dimensional projection. This approach is particularly popular in studies of protein folding, initiated by ideas from the theory of glasses.<sup>116</sup> The description of dynamics in terms of a one-dimensional diffusion equation has often proved useful,<sup>89,90,117,118</sup> although the caveats of the original authors are worth quoting:<sup>116</sup> “we should point out, however, that our assumed dynamics in this model may well be quite unrealistic for actual proteins (although not necessarily for a large class of *simulations* of proteins).”

Most applications actually consider a Smoluchowski equation, which includes additional parameters and a general position dependence for the diffusion coefficient and the average velocity. The resulting drift-diffusion equation is usually written with a friction term corresponding to viscous drag and corresponds to the Fokker-Planck equation for the time evolution of a probability density function associated with particle positions. The drag terms or random forces could arise from variation in solvent viscosity<sup>119–122</sup> but will also subsume the effect of projecting the dynamics onto a low-dimensional space. Even if the projection does not provide a faithful description of some barriers, it may still be possible to apply corrections based on local analysis of the dynamics in the full space, although they may be coordinate dependent.<sup>90</sup> The phenomenological “friction” then includes dimensionality reduction effects inherent in the projection, which generally slow the dynamics when the reaction coordinate does not account for

barriers in the potential energy landscape corresponding to full dimensionality. This effect is sometimes associated with “roughness,” manifested as a position-dependent effective diffusion coefficient, which affects the physical interpretation of this phenomenological parameter. The original barriers on the potential energy surface are therefore reflected in two different ways in a low-dimensional projection. The barriers along the reaction coordinate are still explicit, but barriers in orthogonal degrees of freedom correspond to position-dependent diffusion coefficients. Some groups describe both the explicit and implicit barriers as “roughness.”

The capability of single-molecule fluorescence experiments to probe both folding rates and the time associated with actually making a conformational transition provides detailed tests of dynamics.<sup>123</sup> In simulations, the barriers associated with conformational transitions of a biomolecule change with both implicit and explicit solvent representations. Since these barriers depend on the solvent representation, they are actually correlated directly with the solvent, and we should not necessarily expect that the solute degrees of freedom can be decoupled. The convolution of effects seems likely to be system specific, depending upon whether the time scale for the rate-determining step is well separated from other relaxation processes. It is not obvious whether interpretation of “internal friction” as a less than a first power dependence on the solvent viscosity for the mean first passage and transition path times is equivalent to changes in these conformational barriers.

Computer simulations are likely to play a key role in future work here.<sup>124,125</sup> For example, the interplay of explicit solvent viscosity and conformational transitions over effective torsional barriers has been examined in detail for a small helical protein.<sup>126</sup> The rate-determining pathways between protein configurations in this case are in line with previous results, where the corresponding transition states were calculated using geometry optimisation including all the protein degrees of freedom.<sup>127,128</sup>

A friction constant is explicitly introduced into simulations based upon the Langevin equation, which aim to account for omitted explicit solvent degrees of freedom, which are assumed to equilibrate quickly.<sup>129</sup> Here, the frictional drag is proportional to the velocity on each particle (Stoke’s law), and the resulting model is equivalent to a Fokker-Planck equation.<sup>130</sup> In the simplest formulation, a memoryless noise term, where the noise contributions at different times are uncorrelated, is added to the frictional drag. Expressions for the rate constant that depend upon a position-independent friction coefficient were derived for one degree of freedom by Kramers,<sup>131,132</sup> and various extensions to multidimensional problems<sup>133,134</sup> and generalised friction kernels<sup>135–139</sup> have been described. Here, we also note Kramer’s comment: “we expect the transition state method gives results which are correct, say, within 10% in a rather wide range of  $\eta$ -values,”<sup>131</sup> where  $\eta$  is a viscosity parameter. However, this conclusion may be optimistic, given the assumptions in Kramers’ derivation of separation between fast and slow degrees of freedom, projection of the dynamics onto low dimensionality, and uncorrelated noise.

In the present work, we avoid complications of interpretation due to solvent effects and possible issues associated with

describing dihedral angle rotations<sup>139</sup> by considering a gas phase atomic cluster. Hence, we can focus directly upon the projection of the dynamics onto a single degree of freedom. We therefore disentangle the effect of the projection, from any additional interpretation of friction that arises from stochastic treatments of missing explicit solvent degrees of freedom. The potential energy landscape perspective, based upon construction of kinetic transition networks, does not require or use such reaction coordinates. All degrees of freedom are usually retained, although it is certainly possible to reduce the dimensionality using arbitrary sets of atoms that define local rigid bodies.<sup>48,50,51</sup> Overall rate constants can be extracted based upon unimolecular rate theory involving all degrees of freedom, exploiting either transition state theory formulations<sup>17,29,30,67</sup> or generalised Kramers approaches.<sup>134</sup> The underlying master equation formulation is also the foundation of methods that define states from explicit molecular dynamics simulations. This framework has been used in a number of studies for biomolecules, where it is usually referred to as Markov state modelling.<sup>140–144</sup>

#### IV. SAMPLING A GEOMETRICALLY DEFINED PATHWAY

The basic idea introduced here is to use geometrical pathways to construct potentials of mean force. A Monte Carlo sampling procedure is employed subject to the restriction that configurations must remain within a constraint distance  $d$  of at least one structure saved on a reference pathway.

In the creation of a kinetic transition network<sup>69–71</sup> within the DPS framework, approximate steepest-descent pathways are calculated for every transition state. In the present work, these energy minimisations were performed using a modified version of the limited memory Broyden-Fletcher-Goldfarb-Shanno (L-BFGS) algorithm,<sup>145,146</sup> which is implemented in the GMIN<sup>147</sup> and OPTIM<sup>148</sup> programs. For a composite pathway involving multiple transition states, the individual paths are aligned and joined. Aside from the initial and final states, local minima at the end points of the individual paths will appear twice and are aligned and tested to make sure that any residual distance between the configurations lies below a specified tolerance. Minimising the Euclidean distance between configurations in  $3N$  dimensions for an  $N$ -atom molecule with respect to overall translation and rotation employs a straightforward quaternion algorithm.<sup>149</sup> However, alignment with respect to permutation-inversion isomers may also be necessary, and then an iterative procedure is required. Here, we alternate alignment with respect to overall rotation and translation with permutational optimisation based upon a shortest augmenting path algorithm,<sup>150</sup> as coded in OPTIM.<sup>78</sup> Enantiomers are also considered in each cycle. The sequence of alignment steps can produce a different local minimum in the distance for different initial orientations, and here, we employed up to 1000 initial conditions to ensure that the best solution was almost certainly obtained. A smaller value could safely be used, but the overhead involved is negligible, since the full alignment procedure need only be performed once.

This potential of mean force approach can be used with any suitable selection of configurations from the individual

pathways. The key requirement is that adjacent configurations are not so far apart that they are mutually inaccessible for the given constraint distance  $d$ , which would break ergodicity in the sampling. This condition was checked on initialisation, when the successive configurations for a particular discrete path were read and aligned in sequence, using the iterative procedure described above. After this initial pass, the permutational isomers were fixed, so that subsequent distance checks in the MC procedure needed only to deal with overall translation/rotation. Standard canonical MC runs were then conducted, with the restriction that any proposed steps leading to configurations outside the distance constraint were simply rejected, with the previous configuration recounted to avoid boundary effects.<sup>151</sup>

To improve the efficiency, two further measures were considered. Since the distance check has identified the closest reference configuration,  $n$ , for the proposed configuration  $\mathbf{X}$ , we can use the corresponding potential energy of this reference to construct a bias potential as  $W(\mathbf{X}) = -V_n(\mathbf{X})$ , in the spirit of umbrella sampling.<sup>152</sup> Here,  $V_n(\mathbf{X})$  is the potential energy of reference configuration  $n$ . The biased MC sampling then employs Metropolis accept/reject steps based on the potential  $V(\mathbf{X}) + W(\mathbf{X})$ . The expectation value for an observable,  $O(T)$ , at temperature  $T$  is recovered from the average value in the biased ensemble using the standard result<sup>153</sup>

$$\langle O(T) \rangle = \left\langle O(T) e^{W(\mathbf{X})/k_B T} \right\rangle_W / \left\langle e^{W(\mathbf{X})/k_B T} \right\rangle_W, \quad (1)$$

where the subscript  $W$  indicates an average calculated in the biased ensemble. Subtracting the potential energy of a nearby reference configuration should increase the acceptance probability by effectively flattening the potential energy profile of the path. The accuracy of this approach in the example discussed below was assessed by comparing the results from biased and unbiased sampling, which were in quantitative agreement at convergence. Faster convergence was achieved using biased sampling, as expected.

The objective in the present contribution is to compare potentials of mean force projected onto a geometrical order parameter,  $Q_6$  (see Sec. V), and as a function of the integrated path length,  $s$ . Here,  $s$  is approximated from the step lengths in  $3N$ -dimensional space between the configurations along the reference pathway, where  $N$  is the number of atoms. The bins can have different widths, and the selected reference configurations were checked to ensure all adjacent frames were separated by less than the distance constraint value, so that  $|\mathbf{X}_i - \mathbf{X}_{i+1}| < d$ . In practice, this condition was achieved by setting a relatively small maximum step size in the L-BFGS procedure used to calculate the reference pathway (an order of magnitude less than the smallest  $d$  value considered) and aligning frames from different initial orientations until the separation was less than twice the maximum step size. The configurations obtained by energy minimisation are very close together near the stationary points, so only representatives corresponding to a minimum change in potential energy (or separation) were included.

The potentials of mean force that we aim to compare are Landau free energies obtained from the occupation probabilities of the bins for the integrated path length and the  $Q_6$  order parameter:  $F(s) = -k_B T \ln P(s)$  and  $F(Q_6) = -k_B T \ln P(Q_6)$ .

These probabilities can be obtained simply by accumulating statistics in the MC runs, using Eq. (1) for biased sampling with observables corresponding to the number of visits to either  $s$  or  $Q_6$  bins. Instead of simply counting visits, we accumulate an average value for  $\exp[W(\mathbf{X})/k_B T]$  for each bin.

To accelerate the sampling, separate MC runs were conducted for overlapping segments of the reference pathway. These segments were chosen in terms of blocks of  $b$  sequential reference configurations, with  $c$  overlapping configurations in common between neighbouring blocks. The simulations

for each block are independent and were run on separate processors, so the efficiency gain scales linearly with the number of processors available. The sampling within each block generates the correct relative probabilities for each  $s$  bin, since all the configurations that contribute to each bin are accessible. The overlap condition enables us to combine the statistics from the different blocks in a weighted histogram analysis method (WHAM<sup>154–158</sup>). Here, we optimised the one-dimensional probability distribution for  $P(s)$  by minimising the statistic<sup>157</sup>

$$\chi_{1D}^2 = \sum_r \sum_s N_{rs} [\ln P(s) - \ln P_{rs} Z_r]^2, \quad \text{where} \quad N_{rs} = \sum_{j \in s} 1, \quad (2)$$

$$\text{and} \quad P_{rs} = \frac{N_{rs}}{N_r} \quad (\text{unbiased}) \quad \text{or} \quad P_{rs} = \frac{\sum_{j \in s} \exp[W(\mathbf{X}_j)/k_B T]}{\sum_j \exp[W(\mathbf{X}_j)/k_B T]} \quad (\text{biased}).$$

The sums over  $j$  are for the configurations in the Markov chain obtained for block  $r$ , and the variables are  $P(s)$  and  $Z_r$ , with  $N_r$  is the total number of MC steps for sampling of block  $r$ . Direct minimisation using the modified LBFGS approach was employed with analytical first derivatives for  $\chi_{1D}^2$ <sup>145,146</sup> in terms of  $\ln P(s)$  and  $\ln Z_r$ .

The situation is different for order parameters like  $Q_6$ , where some regions of configuration space that contribute to a particular order parameter bin,  $q$ , may lie outside the block that is sampled in a given run. In this case, the statistics for each run provide the relative probabilities for the order parameter bins within each block,  $P_{rq}$ , which depend upon  $r$ . In this case, we could optimise a joint probability distribution,  $P(s, q)$ , and obtain  $P(q)$  by summing over  $s$ . However, there is a faster alternative that proved to be sufficient for the present purposes. Averages were accumulated for the order parameter within each  $s$  bin as

$$\langle q \rangle_{sr} = \frac{\sum_{j \in s} q(\mathbf{X}_j)}{N_{rs}} \quad (\text{unbiased}) \quad \text{or}$$

$$\langle q \rangle_{sr} = \frac{\sum_{j \in s} q(\mathbf{X}_j) e^{W(\mathbf{X}_j)/k_B T}}{\sum_j e^{W(\mathbf{X}_j)/k_B T}} \quad (\text{biased}).$$

Having solved the one-dimensional optimisation problem for  $P(s)$ , we can then approximate  $P(q) = \sum_s P(s)P(q|s) \sim \sum_s P(s)\delta(\langle q \rangle_{sr} - q)$ . Here, the conditional probability  $P(q|s)$  is estimated using the average value for the  $s$  bin in question. For  $s$  bins contained in overlap regions, there is a choice of two blocks,  $r$ , for the mean value  $\langle q \rangle_{sr}$ , and the results were insensitive to this choice. The average corresponding to the bin with the most visits (larger  $N_{rs}$ ) was used throughout in the present work, although the mean values  $\langle q \rangle_{sr}$  generally gave the same bin for the order parameter, as specified by the delta function. Moments of the order parameter in this approximation can also be calculated. For example, the overall mean value is a sum over the  $q$  values with each one weighted

by the sum of  $P(s)$  probabilities for  $s$  bins with  $q$  averages that lie in the  $q$  bin in question.

Approximate free energy surfaces  $F(s, q)$  were obtained as  $-k_B T \ln P(s)P(q|s)$ , with the conditional probability approximated as above. The resulting surface was visualised by convoluting with a product of Gaussians centred at the two-dimensional grid position corresponding to  $(s, \delta(\langle q \rangle_{sr} - q))$  for each  $s$ . This representation provides a clear picture of how different configurations along the geometrical pathway can contribute to the same value for a more coarse-grained order parameter. Barriers between these configurations would then not be accounted for explicitly in the order parameter projection. Such terms would have to be corrected empirically via position-dependent diffusion constants if dynamics are calculated for this projection.

Results were also compared for averages calculated using the order parameter values for the static reference configurations, instead of the average value for the instantaneous configurations sampled in each  $s$  bin. The resulting probability distributions for the bond order parameter  $Q_6$  exhibited systematic shifts. For example, larger  $Q_6$  values are obtained for structures closer to local minima with fcc character. An illustration is presented in Sec. V for a connection between two adjacent minima that produces a bimodal distribution for  $Q_6$ . Further details of such self-consistency checks are omitted for brevity.

If the blocks are large enough to contain all the possible contributions to each  $q$  bin, which is certainly the case for a single block corresponding to the whole path, then the  $P(q)$  probabilities are recovered directly. This limit was checked for several runs, and quantitative agreement was obtained when the distributions from sufficiently large blocks were properly converged.

## V. RESULTS FOR AN ATOMIC CLUSTER

The benchmark system considered here for illustration is the 38-atom cluster bound by the pairwise additive, isotropic Lennard-Jones (LJ) potential,<sup>160</sup> where the energy is

$$V = 4\epsilon \sum_{i < j} \left[ \left( \frac{\sigma}{r_{ij}} \right)^{12} - \left( \frac{\sigma}{r_{ij}} \right)^6 \right]. \quad (3)$$

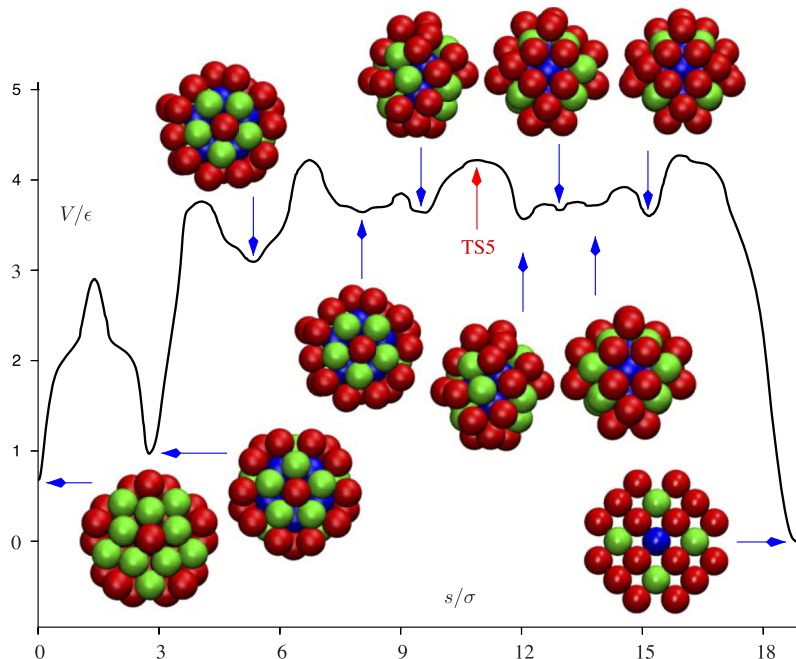
$\epsilon$  and  $2^{1/6}\sigma$  are the pair equilibrium well depth and separation, respectively, and we employ reduced units of energy and distance defined by  $\epsilon$  and  $\sigma$ .

This LJ<sub>38</sub> cluster is an archetypal double-funnel system,<sup>41,82</sup> in terms of competition between competing morphologies based upon Mackay icosahedral packing and structures involving the truncated octahedron, which is based on fcc structure. The organisation of the potential energy landscape is probably best understood in terms of the disconnection graph<sup>81,82</sup> shown in Figure 1. The multifunnel structure has made this system a benchmark for global optimisation,<sup>42</sup> enhanced thermodynamic sampling,<sup>10,11,63,64,159,161–163</sup> and rare event dynamics.<sup>17,29,164</sup> The overall rate constants for interconversion of morphologies have been reported for transitions between the lowest energy local minima in the two funnels.<sup>41</sup> This lumping scheme avoids complications due to internal structure in the funnels. For example, some of the low-lying minima based on icosahedral packing are themselves separated from the lowest-lying  $C_{5v}$  minimum by relatively high barriers. It has been noted that slow dynamics would also be associated with such structure.<sup>165</sup> Hence, this usual grouping scheme provides a simplification, which should be appropriate for experiments that simply distinguish states based upon the underlying packing.

In previous work on atomic clusters, bond-order packing descriptors<sup>166,167</sup> have proved to be very useful in deducing which structural families local configurations belong to.<sup>22,159,168–170</sup> Here, we define

$$Q_l = \left( \frac{4\pi}{2l+1} \sum_{m=-l}^l |\bar{Q}_{lm}|^2 \right)^{1/2}, \quad \text{with}$$

$$\bar{Q}_{lm} = \frac{1}{N_b} \sum_{r_{ij} < r_0} Y_{lm}(\theta_{ij}, \phi_{ij}), \quad (4)$$



where the sum for  $\bar{Q}_{lm}$  is over all the  $N_b$  pairs of atoms with separation,  $r_{ij}$ , less than a nearest-neighbour cutoff condition  $r_0 = 1.391\sigma$ .  $Y_{lm}(\theta, \phi)$  is a spherical harmonic and  $\theta_{ij}$  and  $\phi_{ij}$  are the polar and azimuthal angles of the interatomic vector with respect to an arbitrary coordinate frame. The most useful member of this family for LJ<sub>38</sub> is  $Q_6$ , which takes larger values for the truncated octahedral global minimum than for structures based upon icosahedral packing (Figure 6).

The block size used throughout was 10 frames of the reference pathway, with overlaps of five frames. Very similar results were obtained for alternative choices, and there is clearly scope for optimising these values in future applications. Smooth probability distributions are presented by convolution with normalised Gaussian functions centred on the  $s$  and  $Q_6$  bin values with variances of 0.025 and 0.000 025, respectively. The energetic profile for the selected discrete path is shown in Figure 2. It consists of nine transition states connecting ten minima, as summarised in Table I. The committor probabilities corresponding to the ten minima in this reduced kinetic transition network are plotted as a function of temperature in Figure 3. The fundamental problem with using  $Q_6$  as a reaction coordinate is immediately clear: while the committor probabilities and integrated path length change monotonically from product to reactant,  $Q_6$  does not.

The first step on the overall path involves two low-lying members of the icosahedral region of configuration space, which are separated by a relatively high barrier. The two structures exhibit alternative Mackay and anti-Mackay surface packings.<sup>171,172</sup> They are lumped together in previous analyses of rates for interconversion of morphologies,<sup>17,29,41</sup> but the corresponding structure can easily be resolved in the underlying network.<sup>165</sup> A well-defined minimum appears in  $P(s)$  around  $s = 2.8$  for constraint distances of  $d = 0.4, 0.7$ , and  $1.0$ , over the temperature range  $0.12$ – $0.3$ , as shown in Figure 4. However, the  $Q_6$  order parameter fails to identify this feature; although it discriminates the fcc and icosahedral morphologies

FIG. 2. Relative potential energy  $V$  as a function of the integrated path length  $s$  for an interconversion pathway of the LJ<sub>38</sub> cluster between the lowest energy incomplete Mackay icosahedral structure and the global minimum truncated octahedron. The ten minima corresponding to this nine-step pathway are also illustrated with the atoms coloured according to their contribution to the total energy. The most tightly bound atoms are blue, the least tightly bound are red, with intermediate binding energies in green. TS5 indicates the position of transition state number 5, for reference to Figure 7.

TABLE I. Properties of the minima and transition states on the nine-step pathway analysed for LJ<sub>38</sub>. “Frame” refers to the position of this structure in the discretised set of configurations representing the overall pathway.  $V$  is the potential energy,  $Q_6$  is the bond order parameter, and  $s$  is the integrated path length at which the structure appears.

Frame	Structure	$V/\epsilon$	$Q_6$	$s$
887	MIN	-173.252 378 4	0.13	0.0
827	TS	-171.024 873 0	0.14	1.4
767	MIN	-172.958 633 4	0.13	2.8
711	TS	-170.167 437 6	0.14	4.1
645	MIN	-170.834 772 1	0.15	5.3
580	TS	-169.708 233 8	0.13	6.7
516	MIN	-170.284 399 8	0.15	8.1
465	TS	-170.076 795 9	0.20	9.0
429	MIN	-170.290 420 6	0.20	9.6
371	TS	-169.709 157 3	0.16	10.9
314	MIN	-170.361 742 3	0.12	12.1
287	TS	-170.196 911 4	0.13	12.6
270	MIN	-170.262 952 9	0.14	12.6
246	TS	-170.172 307 6	0.14	13.4
229	MIN	-170.215 482 6	0.13	13.7
189	TS	-170.007 066 7	0.20	14.6
157	MIN	-170.327 349 2	0.25	15.2
123	TS	-169.655 932 0	0.30	15.9
1	MIN	-173.928 426 6	0.57	18.8

quite well, it is not sensitive enough to details of the structure to provide a faithful reflection of the energy profile. Hence, any attempt to analyse dynamics based on the  $F(Q_6)$  potential of mean force will suffer from the projection effects discussed in Sec. III. In contrast, the profiles obtained for  $F(s)$  retain such details of the underlying landscape. The effect of projection can be clearly defined because this system is not subject to the

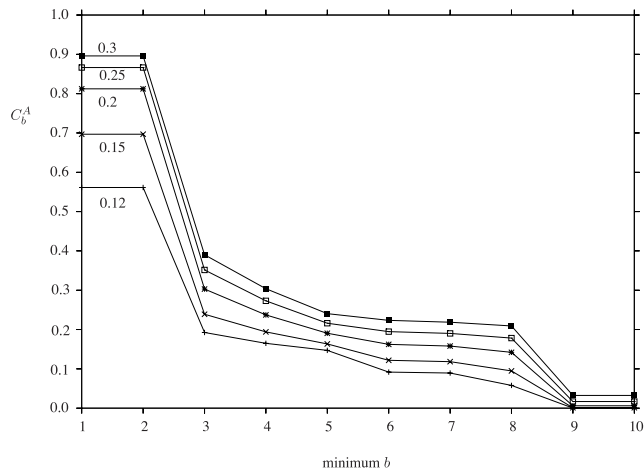


FIG. 3. Commitor probabilities for the ten local minima on the interconversion pathway of LJ<sub>38</sub> corresponding to Figure 2.  $C_b^A$  is the probability that the system will visit the product,  $A$  (minimum 1), before returning to the starting minimum  $b$ , calculated using graph transformation and a sparse linear algebra solver based upon Lower Upper (LU) factorisation.<sup>67,76</sup> The lines joining the points are simply intended to guide the eye. Results are presented for reduced temperatures of  $k_B T / \epsilon = 0.1, 0.15, 0.2, 0.25$ , and  $0.3$ , as marked. It is noteworthy that the variation with temperature is largest in the proximity of the product minimum.

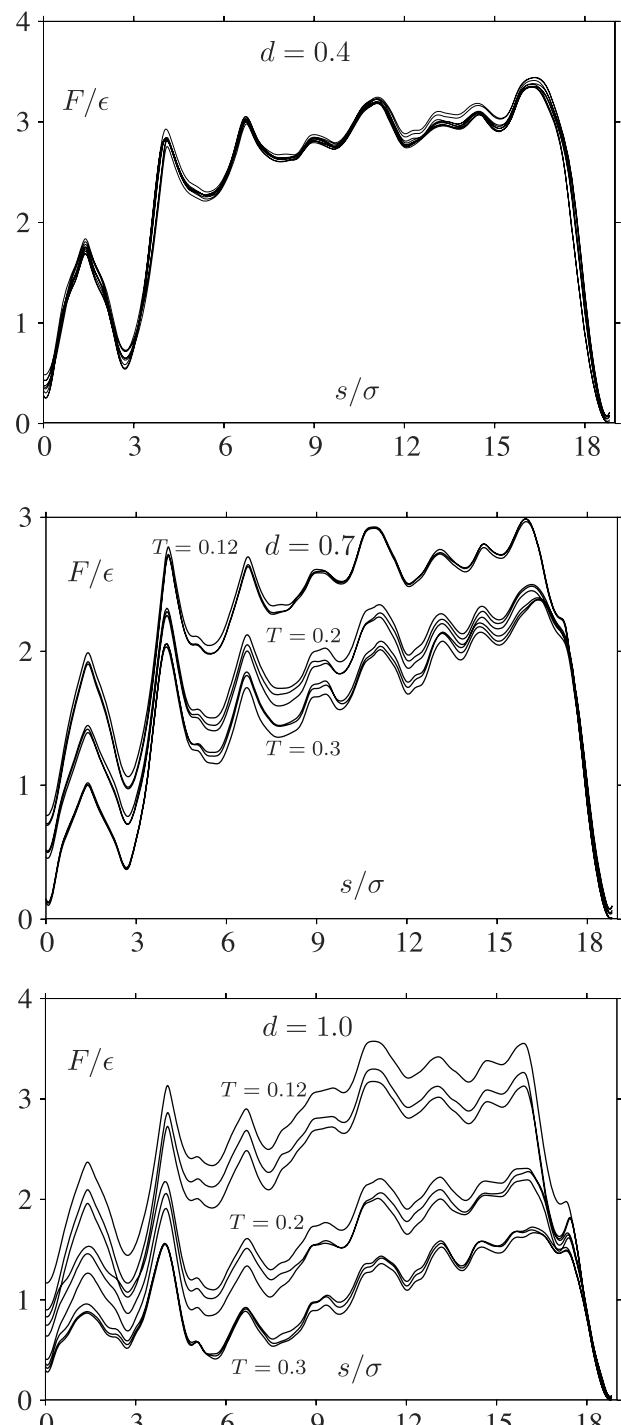


FIG. 4. Free energy  $F$  as a function of the integrated path length  $s$  for a common interconversion pathway of LJ<sub>38</sub>. Results for constraining distances  $d = 0.4, 0.7$ , and  $1.0$  are shown separately, each including temperatures of  $k_B T / \epsilon = 0.12, 0.2$ , and  $0.3$ , with three different starting points for each  $d, T$  combination to check convergence. For  $d = 0.4$ , the nine curves are practically coincident.

“frictional” effects associated with missing degrees of freedom from an environment.

The result of projection is also clear from the  $F(s, Q_6) = -k_B T \ln P(s)P(Q_6|s)$  surfaces illustrated in Figure 5. Gaussian functions with the same variances employed for the one-dimensional visualisations were used to produce smooth surfaces. The double minimum for the two alternative

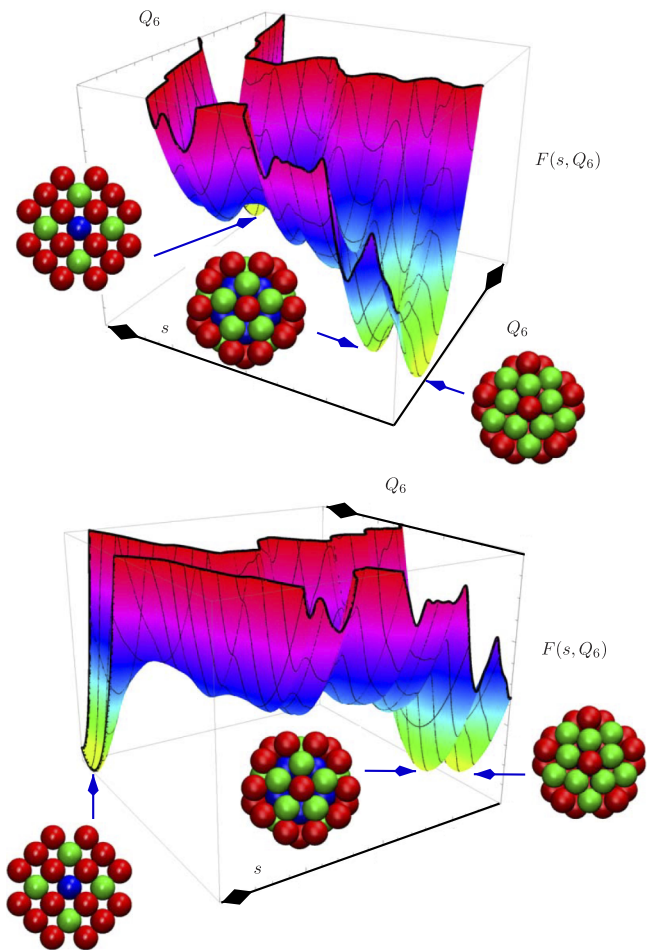


FIG. 5. Two views of the free energy surface obtained from  $-k_B T \ln P(s)$   $P(Q_6|s)$  for constraint distance 0.4 and  $k_B T / \epsilon = 0.12$ . The positions of three low-lying minima are marked.<sup>159</sup>

surface packings is apparent for the  $s$  coordinate. However, when a one-dimensional projection onto  $Q_6$  is employed, the two minima (and the barrier region) are simply averaged over.

The results for  $F(s)$  in Figure 4 exhibit some systematic trends. For  $d = 0.4$ , the shortest constraint distance, there is little temperature dependence. In contrast, for  $d = 1.0$ ,  $F(s)$  shifts systematically to a narrower range as the temperature increases, but the positions of local maxima and minima are preserved. The effects of changing constraint distance and temperature on  $F(Q_6)$  are similar (Figure 6), but the plots are dominated by two deep free energy minima corresponding to  $Q_6$  values around 0.14 and 0.55 for icosahedral and fcc structure, respectively. These minima are consistent with the profiles obtained in previous work using parallel tempering and adaptively biased Monte Carlo.<sup>159</sup> Precise agreement is not expected, since the full configuration space is accessible in the latter calculations. For example, a shallower minimum corresponding to decahedral packing is then observed around  $Q_6 = 2.8$ .<sup>159</sup> For the single pathway examined here, such structure does not arise. One further check was performed to verify that  $F(s)$  approaches  $V(s)$ , the potential energy defined by the reference configurations, at low temperature.

Results for one of the path segments connecting two adjacent minima are shown in Figure 7. This section of the path, corresponding to the fifth transition state in Table I,

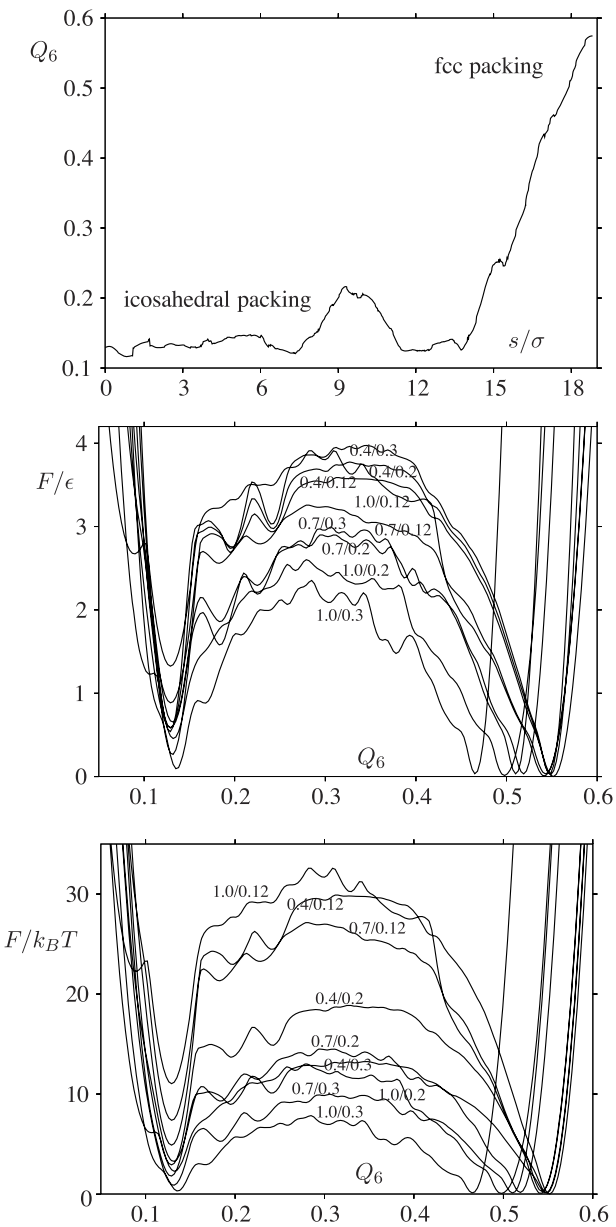


FIG. 6. Top:  $Q_6$  as a function of the configurations characterising an interconversion pathway of LJ<sub>38</sub>. Middle: free energy  $F$  as a function of  $Q_6$  for the same path. The results correspond to constraining distances  $d = 0.4, 0.7$ , and 1.0 and temperatures  $k_B T / \epsilon = 0.12, 0.2$ , and 0.3, as marked on the plots. Bottom: as for the middle plot but illustrating  $F(Q_6)/k_B T$  for comparison with previous work.

is interesting because it exhibits a bimodal distribution for  $Q_6$  (Figure 7). The minima have  $Q_6$  values of 0.20 and 0.12 and are sufficiently similar in energy to have comparable occupation probabilities for the temperature range considered here. This example is selected to illustrate the agreement between  $Q_6$  distributions calculated in different ways. Results are compared for direct visit statistics for the  $Q_6$  bins using a single block containing all the reference configurations, average values of  $Q_6$  for instantaneous and reference configurations for the  $s$  bins weighted by  $P(s)$ , and a harmonic superposition calculation,<sup>1,54–56</sup> which only uses the  $Q_6$  values for the two minima. The distributions agree very well, particularly at this relatively low temperature, where anharmonic effects are small.

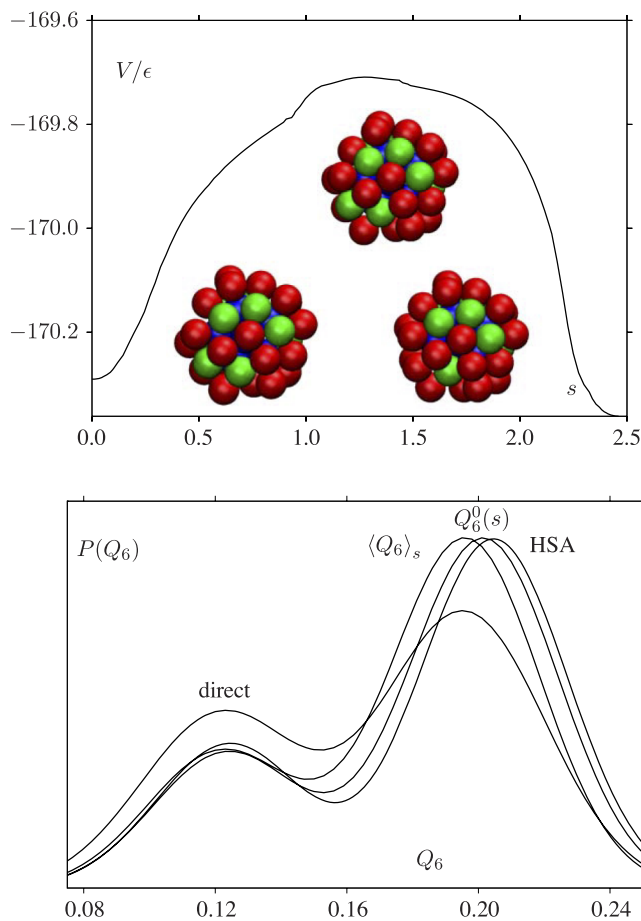


FIG. 7. Analysis of the pathway segment connecting the fifth and sixth minima (see Table I and Figure 2) in  $\text{LJ}_{38}$  for  $d = 0.4$ ,  $k_B T/\epsilon = 0.12$ . Top: the potential energy as a function of the integrated path length; the structures of the three stationary points are illustrated with the same colouring scheme as defined for Figure 2. Bottom: probability distributions calculated in four different ways. “Direct” refers to the distribution based on direct visits for a single block including all the frames. The plots labelled  $\langle Q_6 \rangle_s$  and  $Q_6^0(s)$  were obtained using the mean value of  $Q_6$  in bin  $s$  and the value for the reference configuration corresponding to bin  $s$ , respectively, to approximate  $P(Q_6)$  from  $P(s)$  contributions (see Sec. IV). The plot labelled HSA was obtained using the  $Q_6$  values for the two minima, weighted by their relative occupation probabilities in the harmonic superposition approximation.<sup>1,54–56</sup> A smoothed distribution was obtained by convolution with Gaussian functions centred at the two  $Q_6$  values with a variance of 0.0005.

## VI. CONCLUSIONS

Fitting an effective diffusion constant to reproduce dynamical observables from a low-dimensional representation is a popular approach in molecular science. The variation of this parameter along the corresponding pathway then subsumes projection effects that arise from barriers that are not reproduced by the chosen order parameter. These barriers appear in orthogonal degrees of freedom and are averaged over by the projection. Hence, a smaller value for the effective diffusion constant will be needed to fit the dynamics in such regions.

A clear example is provided for one particular pathway corresponding to the change in morphology of an atomic cluster. In this case, a bond order parameter is relatively successful in reproducing the overall transformation but misses a surface reorganisation associated with a relatively high barrier. In contrast, a profile based on the union of steepest-descent paths between local minima on the potential energy landscape

faithfully reflects the underlying barriers. This result essentially follows from geometry: the steepest-descent paths should correspond to minimum potential energy in the orthogonal degrees of freedom.

Approximate steepest-descent paths are used to define the adjacency of local minima from the transition states that connect them in the construction of kinetic transition networks.<sup>69–71,173</sup> Within this computational potential energy landscape approach, overall rates are usually extracted using unimolecular rate theory based upon all degrees of freedom, which is essentially a master equation formulation.<sup>17,174</sup> This is the basis of the discrete path sampling<sup>17,29,30,67</sup> framework for analysis of rare event dynamics. Since the discrete paths can all be identified and analysed from the static network, there is an opportunity to use them to guide the construction of simplified lower-dimensional representations of the dynamics more systematically in future work.

Coarse-graining global thermodynamics and kinetics using local minima, transition states, and the steepest-descent paths that connect them provides a purely geometrical basis for the prediction of emergent observable phenomena from the potential energy landscape. For example, we can associate distinct *well* and *landscape* contributions to the entropy from the basins defining individual local minima and the distribution of local minima on the landscape. Similarly, entropic contributions to the overall kinetics can be analysed in terms of individual discrete paths connecting local minima via transition states and the distribution of discrete paths. For example, the number of kinetically relevant discrete paths will generally increase with temperature, and this effect has been examined in previous work.<sup>17,29</sup> Combining this insight with more accurate treatment of dynamics would provide an attractive way to analyse rare events.

The application presented here explicitly avoids any complications due to solvent effects, to focus directly on the consequences of dimensionality reduction. In future work, this approach could be applied to biomolecules with both implicit and explicit solvents. For explicit solvent, such analysis is likely to be complicated by the complexity associated with the additional degrees of freedom. Nevertheless, there may be opportunities to gain fresh insight from the potential energy landscape approach. For example, one interpretation of secondary structure kinetics when solvent viscosity is modified explicitly in experiments requires a correlation between barrier height and curvature.<sup>175</sup> This correlation is indeed expected from catastrophe theory if the path length is roughly constant,<sup>1,176</sup> a result that has been investigated quantitatively for atomic and molecular clusters in previous work.

## ACKNOWLEDGMENTS

I am very grateful to Dr. Jacob Stevenson for discussions concerning weighted histogram analysis and for checking the extraction of probability distributions from visits statistics independently using the PELE package.<sup>177</sup> I am also very grateful to Professor Bill Eaton, Dr. David de Sancho, Dr. Robert Best, and Boris Fackovec for comments on the original manuscript and to the referees for some helpful suggestions. This work was supported by the ERC and the EPSRC.

- <sup>1</sup>D. J. Wales, *Energy Landscapes* (Cambridge University Press, Cambridge, 2003).
- <sup>2</sup>R. H. Swendsen and J.-S. Wang, *Phys. Rev. Lett.* **57**, 2607 (1986).
- <sup>3</sup>D. Earl and M. W. Deem, *Phys. Chem. Chem. Phys.* **7**, 3910 (2005).
- <sup>4</sup>R. Zhou and B. J. Berne, *J. Chem. Phys.* **107**, 9185 (1997).
- <sup>5</sup>U. H. E. Hansmann and Y. Okamoto, *Curr. Opin. Struct. Biol.* **9**, 177 (1999).
- <sup>6</sup>F. Wang and D. P. Landau, *Phys. Rev. Lett.* **86**, 2050 (2001).
- <sup>7</sup>W. Watanabe and W. P. Reinhardt, *Phys. Rev. Lett.* **65**, 3301 (1990).
- <sup>8</sup>I. Andricioaei, J. E. Straub, and A. F. Voter, *J. Chem. Phys.* **114**, 6994 (2001).
- <sup>9</sup>J. Kim, J. E. Straub, and T. Keyes, *Phys. Rev. Lett.* **97**, 050601 (2006).
- <sup>10</sup>V. A. Sharapov and V. A. Mandelshtam, *J. Phys. Chem. A* **111**, 10284 (2007).
- <sup>11</sup>V. A. Sharapov, D. Meluzzi, and V. A. Mandelshtam, *Phys. Rev. Lett.* **98**, 105701 (2007).
- <sup>12</sup>J. Kim, T. Keyes, and J. E. Straub, *J. Chem. Phys.* **135**, 061103 (2011).
- <sup>13</sup>J. Kim, J. E. Straub, and T. Keyes, *J. Phys. Chem. B* **116**, 8646 (2012).
- <sup>14</sup>P. J. Ortoleva, T. Keyes, and M. Tuckerman, *J. Phys. Chem. B* **116**, 8335 (2012).
- <sup>15</sup>G. A. Huber and S. Kim, *Biophys. J.* **70**, 97 (1996).
- <sup>16</sup>D. Bhatt, B. W. Zhang, and D. M. Zuckerman, *J. Chem. Phys.* **133**, 014110 (2010).
- <sup>17</sup>D. J. Wales, *Mol. Phys.* **100**, 3285 (2002).
- <sup>18</sup>C. Dellago, P. G. Bolhuis, and D. Chandler, *J. Chem. Phys.* **108**, 9236 (1998).
- <sup>19</sup>D. Passerone and M. Parrinello, *Phys. Rev. Lett.* **87**, 108302 (2001).
- <sup>20</sup>W. E, W. Ren, and E. Vanden-Eijnden, *Phys. Rev. B* **66**, 052301 (2002).
- <sup>21</sup>S. T. Chill, J. Stevenson, V. Ruehle, C. Shang, P. Xiao, J. D. Farrell, D. J. Wales, and G. Henkelman, *J. Chem. Theory Comput.* **10**, 5476 (2014).
- <sup>22</sup>F. Calvo, *Mol. Phys.* **100**, 3421 (2002).
- <sup>23</sup>K. Arora and C. L. Brooks, *Proc. Natl. Acad. Sci. U. S. A.* **104**, 18496 (2007).
- <sup>24</sup>P. I. Zhuravlev, S. Wu, D. A. Potocyan, M. Rubinstein, and G. A. Papoian, *Methods* **52**, 115 (2010).
- <sup>25</sup>D. A. Potocyan, P. I. Zhuravlev, and G. A. Papoian, *J. Phys. Chem. B* **116**, 1709 (2012).
- <sup>26</sup>P. Tao, A. J. Sodt, Y. Shao, G. König, and B. R. Brooks, *J. Chem. Theory Comput.* **10**, 4198 (2014).
- <sup>27</sup>W. E, W. Ren, and E. Vanden-Eijnden, *J. Phys. Chem. B* **109**, 6688 (2005).
- <sup>28</sup>E. Vanden-Eijnden and M. Venturoli, *J. Chem. Phys.* **130**, 194101 (2009).
- <sup>29</sup>D. J. Wales, *Mol. Phys.* **102**, 891 (2004).
- <sup>30</sup>D. J. Wales, *Int. Rev. Phys. Chem.* **25**, 237 (2006).
- <sup>31</sup>W. E and E. Vanden-Eijnden, *J. Stat. Phys.* **123**, 503 (2006).
- <sup>32</sup>P. Metzner, C. Schutte, and E. Vanden-Eijnden, *J. Chem. Phys.* **125**, 084110 (2006).
- <sup>33</sup>P. Metzner, C. Schütte, and E. Vanden-Eijnden, *Multiscale Model. Simul.* **7**, 1192 (2009).
- <sup>34</sup>Z. Li and H. A. Scheraga, *Proc. Natl. Acad. Sci. U. S. A.* **84**, 6611 (1987).
- <sup>35</sup>D. J. Wales and J. P. K. Doye, *J. Phys. Chem. A* **101**, 5111 (1997).
- <sup>36</sup>D. J. Wales and H. A. Scheraga, *Science* **285**, 1368 (1999).
- <sup>37</sup>D. Aseno, J. D. Stevenson, D. J. Wales, and D. Frenkel, *J. Phys. Chem. B* **117**, 12717 (2013).
- <sup>38</sup>J. T. Ngo, J. Marks, and M. Karplus, in *The Protein Folding Problem and Tertiary Structure Prediction*, edited by K. Merz and S. L. Grand (Birkhäuser, Boston, 1994), pp. 433–506.
- <sup>39</sup>J. D. Bryngelson, J. N. Onuchic, N. D. Soccia, and P. G. Wolynes, *Proteins: Struct., Funct., Bioinf.* **21**, 167 (1995).
- <sup>40</sup>J. N. Onuchic, Z. Luthey-Schulten, and P. G. Wolynes, *Annu. Rev. Phys. Chem.* **48**, 545 (1997).
- <sup>41</sup>J. P. K. Doye, M. A. Miller, and D. J. Wales, *J. Chem. Phys.* **110**, 6896 (1999).
- <sup>42</sup>M. T. Oakley, R. L. Johnston, and D. J. Wales, *Phys. Chem. Chem. Phys.* **15**, 3965 (2013).
- <sup>43</sup>D. J. Wales, *Chem. Phys. Lett.* **285**, 330 (1998).
- <sup>44</sup>D. Schebarchov and D. J. Wales, *J. Chem. Phys.* **139**, 221101 (2013).
- <sup>45</sup>D. Schebarchov and D. J. Wales, *Phys. Rev. Lett.* **113**, 156102 (2014).
- <sup>46</sup>C. Tsallis, *J. Stat. Phys.* **52**, 479 (1988).
- <sup>47</sup>C. Shang and D. J. Wales, *J. Chem. Phys.* **141**, 071101 (2014).
- <sup>48</sup>V. Rühle, H. Kusumaatmaja, D. Chakrabarti, and D. J. Wales, *J. Chem. Theory Comput.* **9**, 4026 (2013).
- <sup>49</sup>D. Chakrabarti, H. Kusumaatmaja, V. Ruhle, and D. J. Wales, *Phys. Chem. Chem. Phys.* **16**, 5014 (2014).
- <sup>50</sup>K. Mochizuki, C. S. Whittleston, S. Somani, H. Kusumaatmaja, and D. J. Wales, *Phys. Chem. Chem. Phys.* **16**, 2842 (2014).
- <sup>51</sup>H. Kusumaatmaja, C. S. Whittleston, and D. J. Wales, *J. Chem. Theory Comput.* **8**, 5159 (2012).
- <sup>52</sup>D. J. Wales, *Philos. Trans. R. Soc., A* **363**, 357 (2005).
- <sup>53</sup>D. Chakrabarti and D. Wales, *Phys. Chem. Chem. Phys.* **11**, 1970 (2009).
- <sup>54</sup>F. H. Stillinger and T. A. Weber, *Science* **225**, 983 (1984).
- <sup>55</sup>D. J. Wales, *Mol. Phys.* **78**, 151 (1993).
- <sup>56</sup>F. H. Stillinger, *Science* **267**, 1935 (1995).
- <sup>57</sup>B. Strodel and D. J. Wales, *Chem. Phys. Lett.* **466**, 105 (2008).
- <sup>58</sup>P. G. Mezey, *Theor. Chim. Acta* **58**, 309 (1981).
- <sup>59</sup>P. G. Mezey, *Potential Energy Hypersurfaces* (Elsevier, Amsterdam, 1987).
- <sup>60</sup>S. Martiniani, J. D. Stevenson, D. J. Wales, and D. Frenkel, *Phys. Rev. X* **4**, 031034 (2014).
- <sup>61</sup>J. Skilling, *Bayesian Anal.* **1**, 833 (2006).
- <sup>62</sup>H. Fukunishi, O. Watanabe, and S. Takada, *J. Chem. Phys.* **116**, 9058 (2002).
- <sup>63</sup>V. A. Mandelshtam, P. A. Frantsuzov, and F. Calvo, *J. Phys. Chem. A* **110**, 5326 (2006).
- <sup>64</sup>D. J. Wales, *Chem. Phys. Lett.* **584**, 1 (2013).
- <sup>65</sup>D. Earl and M. W. Deem, *Phys. Chem. Chem. Phys.* **7**, 3910 (2005).
- <sup>66</sup>J. Geyer, in *Computing Science and Statistics, Proceedings of the 23rd Symposium on the Interface*, American Statistical Association, New York, 1991, p. 156.
- <sup>67</sup>D. J. Wales, *J. Chem. Phys.* **130**, 204111 (2009).
- <sup>68</sup>F. Rao and A. Caflisch, *J. Mol. Biol.* **342**, 299 (2004).
- <sup>69</sup>F. Noé and S. Fischer, *Curr. Opin. Struct. Biol.* **18**, 154 (2008).
- <sup>70</sup>D. Prada-Gracia, J. Gómez-Gardenes, P. Echenique, and F. Fernando, *PLoS Comput. Biol.* **5**, e1000415 (2009).
- <sup>71</sup>D. J. Wales, *Curr. Opin. Struct. Biol.* **20**, 3 (2010).
- <sup>72</sup>D. A. Evans and D. J. Wales, *J. Chem. Phys.* **118**, 3891 (2003).
- <sup>73</sup>J. M. Carr and D. J. Wales, *J. Chem. Phys.* **123**, 234901 (2005).
- <sup>74</sup>J. M. Carr and D. J. Wales, *J. Phys. Chem. B* **112**, 8760 (2008).
- <sup>75</sup>J. M. Carr and D. J. Wales, *Phys. Chem. Chem. Phys.* **11**, 3341 (2009).
- <sup>76</sup>J. D. Stevenson and D. J. Wales, *J. Chem. Phys.* **141**, 041104 (2014).
- <sup>77</sup>K. J. Laidler, *Chemical Kinetics* (Harper & Row, New York, 1987).
- <sup>78</sup>D. J. Wales and J. M. Carr, *J. Chem. Theory Comput.* **8**, 5020 (2012).
- <sup>79</sup>F. H. Stillinger and T. A. Weber, *Phys. Rev. A* **25**, 978 (1982).
- <sup>80</sup>D. J. Wales and J. P. K. Doye, *J. Chem. Phys.* **119**, 12409 (2003).
- <sup>81</sup>O. M. Becker and M. Karplus, *J. Chem. Phys.* **106**, 1495 (1997).
- <sup>82</sup>D. J. Wales, M. A. Miller, and T. R. Walsh, *Nature* **394**, 758 (1998).
- <sup>83</sup>V. K. de Souza and D. J. Wales, *J. Chem. Phys.* **129**, 164507 (2008).
- <sup>84</sup>J. P. K. Doye and D. J. Wales, *J. Chem. Phys.* **111**, 11070 (1999).
- <sup>85</sup>B. Friedrich, Z. Herman, R. Zahradník, and Z. Havlas, *Adv. Quantum Chem.* **19**, 247 (1988).
- <sup>86</sup>A. Banerjee and N. P. Adams, *Int. J. Quantum Chem.* **43**, 855 (1992).
- <sup>87</sup>D. J. Wales, *J. Chem. Phys.* **113**, 3926 (2000).
- <sup>88</sup>W. Quapp, *J. Chem. Phys.* **114**, 609 (2001).
- <sup>89</sup>N. D. Soccia, J. N. Onuchic, and P. G. Wolynes, *J. Chem. Phys.* **104**, 5860 (1996).
- <sup>90</sup>R. B. Best and G. Hummer, *Proc. Natl. Acad. Sci. U. S. A.* **107**, 1088 (2010).
- <sup>91</sup>E. R. Henry, R. B. Best, and W. A. Eaton, *Proc. Natl. Acad. Sci. U. S. A.* **110**, 17880 (2013).
- <sup>92</sup>G. Hummer, *J. Chem. Phys.* **120**, 516 (2004).
- <sup>93</sup>R. B. Best and G. Hummer, *Proc. Natl. Acad. Sci. U. S. A.* **102**, 6732 (2005).
- <sup>94</sup>R. B. Best and G. Hummer, *Phys. Chem. Chem. Phys.* **13**, 16902 (2011).
- <sup>95</sup>L. Onsager, *Phys. Rev.* **54**, 554 (1938).
- <sup>96</sup>A. Ma and A. R. Dinner, *J. Phys. Chem. B* **109**, 6769 (2005).
- <sup>97</sup>B. Qi, S. Muff, A. Caflisch, and A. R. Dinner, *J. Phys. Chem. B* **114**, 6979 (2010).
- <sup>98</sup>Y. M. Rhee and V. S. Pande, *J. Phys. Chem. B* **109**, 6780 (2005).
- <sup>99</sup>W. E, W. Ren, and E. Vanden-Eijnden, *Chem. Phys. Lett.* **413**, 242 (2005).
- <sup>100</sup>G. Cicotti, R. Kapral, and E. Vanden-Eijnden, *ChemPhysChem* **6**, 1809 (2005).
- <sup>101</sup>M. J. Morelli, S. Tanase-Nicola, R. J. Allen, and P. R. t. Wolde, *Biophys. J.* **94**, 3413 (2008).
- <sup>102</sup>A. K. Faradjian and R. Elber, *J. Chem. Phys.* **120**, 10880 (2004).
- <sup>103</sup>S. Kirmizialtin and R. Elber, *J. Phys. Chem. A* **115**, 6137 (2011).
- <sup>104</sup>P. G. Bolhuis, *J. Phys.: Condens. Matter* **15**, S113 (2002).
- <sup>105</sup>B. Peters and B. L. Trout, *J. Chem. Phys.* **125**, 054108 (2006).
- <sup>106</sup>E. E. Borrero and F. A. Escobedo, *J. Chem. Phys.* **127**, 164101 (2007).
- <sup>107</sup>S. L. Quaytman and S. D. Schwartz, *Proc. Natl. Acad. Sci. U. S. A.* **104**, 12253 (2007).
- <sup>108</sup>B. Peters, G. T. Beckham, and B. L. Trout, *J. Chem. Phys.* **127**, 034109 (2007).
- <sup>109</sup>J. Juraszek and P. G. Bolhuis, *Biophys. J.* **95**, 4246 (2008).

- <sup>110</sup>S. V. Krivov and M. Karplus, *Proc. Natl. Acad. Sci. U. S. A.* **105**, 13841 (2008).
- <sup>111</sup>C. Velez-Vega, E. E. Borrero, and F. A. Escobedo, *J. Chem. Phys.* **130**, 225101 (2009).
- <sup>112</sup>W. Lechner, J. Rogal, J. Juraszek, B. Ensing, and P. G. Bolhuis, *J. Chem. Phys.* **133**, 174110 (2010).
- <sup>113</sup>P. V. Banushkina and S. V. Krivov, *J. Chem. Theory Comput.* **9**, 5257 (2013).
- <sup>114</sup>P. Májek and R. Elber, *J. Chem. Theory Comput.* **6**, 1805 (2010).
- <sup>115</sup>B. W. Zhang, D. Jasnow, and D. M. Zuckerman, *Proc. Natl. Acad. Sci. U. S. A.* **104**, 18043 (2007).
- <sup>116</sup>J. D. Bryngelson and P. G. Wolynes, *J. Phys. Chem.* **93**, 6902 (1989).
- <sup>117</sup>C. J. Camacho and D. Thirumalai, *Proc. Natl. Acad. Sci. U. S. A.* **90**, 6369 (1993).
- <sup>118</sup>S. S. Plotkin and P. G. Wolynes, *Phys. Rev. Lett.* **80**, 5015 (1998).
- <sup>119</sup>D. Beece, L. Eisenstein, H. Frauenfelder, D. Good, M. C. Marden, L. Reinisch, A. H. Reynolds, L. B. Sorensen, and K. T. Yue, *Biochemistry* **19**, 5147 (1980).
- <sup>120</sup>A. Ansari, C. M. Jones, E. R. Henry, J. Hofrichter, and W. A. Eaton, *Science* **256**, 1796 (1992).
- <sup>121</sup>T. Cellmer, E. R. Henry, J. Hofrichter, and W. A. Eaton, *Proc. Natl. Acad. Sci. U. S. A.* **105**, 18320 (2008).
- <sup>122</sup>S. J. Hagen, *Curr. Protein Pept. Sci.* **11**, 385 (2010).
- <sup>123</sup>H. S. Chung and W. A. Eaton, *Nature* **502**, 685688 (2013).
- <sup>124</sup>J. C. F. Schulz, L. Schmidt, R. B. Best, J. Dzubiella, and R. R. Netz, *J. Am. Chem. Soc.* **134**, 6273 (2012).
- <sup>125</sup>I. Echeverria, D. E. Makarov, and G. A. Papoian, *J. Am. Chem. Soc.* **136**, 8708 (2014).
- <sup>126</sup>D. de Sancho, A. Sirur, and R. B. Best, *Nat. Commun.* **5**, 1 (2014).
- <sup>127</sup>P. N. Mortenson and D. J. Wales, *J. Chem. Phys.* **114**, 6443 (2001).
- <sup>128</sup>P. N. Mortenson, D. A. Evans, and D. J. Wales, *J. Chem. Phys.* **117**, 1363 (2002).
- <sup>129</sup>D. Chandler, *Introduction to Modern Statistical Mechanics* (Oxford University Press, Oxford, 1987).
- <sup>130</sup>N. G. van Kampen, *Stochastic Processes in Physics and Chemistry* (North-Holland, Amsterdam, 1981).
- <sup>131</sup>H. A. Kramers, *Physica* **7**, 284 (1940).
- <sup>132</sup>P. Hänggi, P. Talkner, and M. Borkovec, *Rev. Mod. Phys.* **62**, 251 (1990).
- <sup>133</sup>J. Langer, *Ann. Phys.* **54**, 258 (1969).
- <sup>134</sup>A. M. Berezhkovskii, E. Pollak, and V. Y. Zitserman, *J. Chem. Phys.* **97**, 2422 (1992).
- <sup>135</sup>R. F. Grote and J. T. Hynes, *J. Chem. Phys.* **73**, 2715 (1980).
- <sup>136</sup>R. F. Grote and J. T. Hynes, *J. Chem. Phys.* **74**, 4465 (1981).
- <sup>137</sup>R. F. Grote and J. T. Hynes, *J. Chem. Phys.* **75**, 2191 (1981).
- <sup>138</sup>A. Nitzan, *J. Chem. Phys.* **86**, 2734 (1987).
- <sup>139</sup>J. Portman, S. Takada, and P. G. Wolynes, *J. Chem. Phys.* **114**, 5069 (2001).
- <sup>140</sup>N. Singhal, C. D. Snow, and V. S. Pande, *J. Chem. Phys.* **121**, 415 (2004).
- <sup>141</sup>J. D. Chodera, K. A. Dill, N. Singhal, V. S. Pande, W. C. Swope, and J. W. Pitera, *J. Chem. Phys.* **126**, 155101 (2007).
- <sup>142</sup>G. R. Bowman, K. A. Beauchamp, G. Boxer, and V. S. Pande, *J. Chem. Phys.* **131**, 124101 (2009).
- <sup>143</sup>J. H. Prinz, H. Wu, M. Sarich, B. Keller, M. Senne, M. Held, J. D. Chodera, C. Schutte, and F. Noe, *J. Chem. Phys.* **134**, 174105 (2011).
- <sup>144</sup>T. J. Lane, G. R. Bowman, K. Beauchamp, V. A. Voelz, and V. S. Pande, *J. Am. Chem. Soc.* **133**, 18413 (2011).
- <sup>145</sup>J. Nocedal, *Math. Comput.* **35**, 773 (1980).
- <sup>146</sup>D. C. Liu and J. Nocedal, *Math. Program.* **45**, 503 (1989).
- <sup>147</sup>D. J. Wales, “GMIN: A program for basin-hopping global optimisation and basin-sampling thermodynamics,” online at <http://www-wales.ch.cam.ac.uk/software.html>.
- <sup>148</sup>D. J. Wales, “OPTIM: A program for optimizing geometries and calculating reaction pathways,” online at <http://www-wales.ch.cam.ac.uk/OPTIM/>.
- <sup>149</sup>S. K. Kearsley, *Acta Crystallogr., Sect. A* **45**, 208 (1989).
- <sup>150</sup>R. Jonker and A. Volgenant, *Computing* **38**, 325 (1987).
- <sup>151</sup>B. J. Schulz, K. Binder, M. Müller, and D. P. Landau, *Phys. Rev. E* **67**, 067102 (2003).
- <sup>152</sup>G. M. Torrie and J. P. Valleau, *Chem. Phys. Lett.* **28**, 578 (1974).
- <sup>153</sup>D. Frenkel and B. Smit, *Understanding Molecular Simulation*, 2nd ed. (Academic Press, London, 2002).
- <sup>154</sup>A. M. Ferrenberg and R. H. Swendsen, *Phys. Rev. Lett.* **61**, 2635 (1988).
- <sup>155</sup>A. M. Ferrenberg and R. H. Swendsen, *Phys. Rev. Lett.* **63**, 1195 (1989).
- <sup>156</sup>P. Labastie and R. L. Whetten, *Phys. Rev. Lett.* **65**, 1567 (1990).
- <sup>157</sup>S. Weerasinghe and F. G. Amar, *J. Chem. Phys.* **98**, 4967 (1993).
- <sup>158</sup>F. Calvo and P. Labastie, *Chem. Phys. Lett.* **247**, 395 (1995).
- <sup>159</sup>F. Calvo, *Phys. Rev. E* **82**, 046703 (2010).
- <sup>160</sup>J. E. Jones and A. E. Ingham, *Proc. R. Soc. A* **107**, 636 (1925).
- <sup>161</sup>J. P. Neirotti, F. Calvo, D. L. Freeman, and J. D. Doll, *J. Chem. Phys.* **112**, 10340 (2000).
- <sup>162</sup>F. Calvo, J. P. Neirotti, D. L. Freeman, and J. D. Doll, *J. Chem. Phys.* **112**, 10350 (2000).
- <sup>163</sup>R. M. Sehgal, D. Maroudas, and D. M. Ford, *J. Chem. Phys.* **140**, 104312 (2014).
- <sup>164</sup>M. Picciani, M. Athenes, J. Kurchan, and J. Tailleur, *J. Chem. Phys.* **135**, 034108 (2011).
- <sup>165</sup>S. V. Krivov and M. Karplus, *J. Phys. Chem. B* **110**, 12689 (2006).
- <sup>166</sup>P. J. Steinhardt, D. R. Nelson, and M. Ronchetti, *Phys. Rev. B* **28**, 784 (1983).
- <sup>167</sup>J. S. van Duijneveldt and D. Frenkel, *J. Chem. Phys.* **96**, 4655 (1992).
- <sup>168</sup>R. M. Lynden-Bell and D. J. Wales, *J. Chem. Phys.* **101**, 1460 (1994).
- <sup>169</sup>P. Poulaing, F. Calvo, R. Antoine, M. Broyer, and P. Dugourd, *Phys. Rev. E* **73**, 056704 (2006).
- <sup>170</sup>V. A. Mandelshtam and P. A. Frantsuzov, *J. Chem. Phys.* **124**, 204511 (2006).
- <sup>171</sup>D. J. Wales, L. J. Munro, and J. P. K. Doye, *J. Chem. Soc., Dalton Trans.* **1996**, 611.
- <sup>172</sup>J. P. K. Doye, M. A. Miller, and D. J. Wales, *J. Chem. Phys.* **111**, 8417 (1999).
- <sup>173</sup>G. C. Boulougouis and D. N. Theodorou, *J. Chem. Phys.* **127**, 084903 (2007).
- <sup>174</sup>N. P. Kopsias and D. N. Theodorou, *J. Chem. Phys.* **109**, 8573 (1998).
- <sup>175</sup>G. S. Jas, W. A. Eaton, and J. Hofrichter, *J. Phys. Chem. B* **105**, 261 (2001).
- <sup>176</sup>D. J. Wales, *Science* **293**, 2067 (2001).
- <sup>177</sup>See <https://github.com/pele-python/pele> for Pele: Python energy landscape explorer.